Manuscript Details

Manuscript number	COST_2018_2284
Title	Experimental study of torsional strengthening on thin walled tubular reinforced concrete structures using NSM-CFRP laminates
Article type	Full Length Article

Abstract

Although the use of near surface mounted (NSM) reinforcement for shear and flexural strengthening of reinforced concrete (RC) structures has been examined extensively in the past twenty years, its performance as torsional strengthening solution has never been assessed. This paper presents an experimental program on the use of NSM carbon fibre reinforced polymer (CFRP) laminates to enhance the torsional behaviour of RC thin walled tubular elements. Six specimens were tested as part of this work, including two reference specimens and the remaining four strengthened with different configurations of longitudinal and transverse CFRP laminates. The research shows that the addition of NSM CFRP laminates is very effective in increasing the torsional moment carrying capacity, stiffness and torsional deformability, and arresting the crack propagation, with imperceptible alteration of the geometry of the strengthened element.

Keywords	Torsional strengthening, near surface mounted technique (NSM), carbon fibre reinforced polymer (CFRP)

Corresponding Author	Chandan Gowda
Order of Authors	Chandan Gowda, Joaquim Barros, Maurizio Guadagnini

Suggested reviewers	A Deifalla, Abdeldjelil Belarbi, Constantin Chalioris

Submission Files Included in this PDF

File Name [File Type]

CoverLetter.doc [Cover Letter]

ChandanEtAl_Text.docx [Manuscript File]

ChandanEtAl_Figures.docx [Figure]

ChandanEtAl_Tables.docx [Table]

To view all the submission files, including those not included in the PDF, click on the manuscript title on your EVISE Homepage, then click 'Download zip file'.

Universidade do Minho
Escola de Engenharia

To the Editor of the Composite Structures Journal

July 5th, 2018

Dear Editor,

I am submitting the manuscript entitled "Experimental study of torsional strengthening no thin walled tubular reinforced concrete structures using NSM-CFRP laminates" by ***Chandan Gowda, Joaquim Barros*** and ***Maurizio Guadagnini*** for consideration of publication in the Composite Structures Journal.

This manuscript describes the experimental work carried out on torsional strengthening of thin walled tubular reinforced concrete beams, with near surface mounted (NSM) technique using carbon fibre reinforced polymer (CFRP) laminates. It consists of testing 6 beams (2 reference and 4 strengthened beams), with different reinforcement configuration of longitudinal and transverse CFRP reinforcement ratios. The results conclude that the proposed strengthening configurations provide very good increase in torsional moment carrying capacity, torsional angle of rotation, arrest in crack propagation and effective utilization of the strengthening CFRP material.

This manuscript describes the Authors' original work. It has not been published elsewhere and is not under consideration by another journal. All the authors approved the manuscript and agree with this submission. No conflict of interest to declare.

Thank you very much for your consideration.
Yours Sincerely,

Chandan Chinnagir Gowda

(Corresponding Author)

Early Stage Researcher/ PhD student

Department of Civil Engineering, ISISE, University of Minho

Campus de Azurém, 4800-058 Guimarães, PORTUGAL

Cel. Ph.: +351 919210773

Email: chandu627@gmail.com

Experimental study of torsional strengthening on thin walled tubular reinforced concrete structures using NSM-CFRP laminates

Chandan C. Gowda [a*], Joaquim A. O. Barros [a], Maurizio Guadagnini [b]

[a] *chandu627@gmail.com, barros@civil.uminho.pt, ISISE, Department of Civil engineering, University of Minho, Campus de Azurém, Guimarães 4800 158, Portugal*

[b] *m.guadagnini@sheffield.ac.uk, Department of Civil and Structural engineering, The University of Sheffield, Sir Fredrik Mappin building, Mapping street, Sheffield S1 3JD, UK*

Abstract

Although the use of near surface mounted (NSM) reinforcement for shear and flexural strengthening of reinforced concrete (RC) structures has been examined extensively in the past twenty years, its performance as torsional strengthening solution has never been assessed. This paper presents an experimental program on the use of NSM carbon fibre reinforced polymer (CFRP) laminates to enhance the torsional behaviour of RC thin walled tubular elements. Six specimens were tested as part of this work, including two reference specimens and the remaining four strengthened with different configurations of longitudinal and transverse CFRP laminates. The research shows that the addition of NSM CFRP laminates is very effective in increasing the torsional moment carrying capacity, stiffness and torsional deformability, and arresting the crack propagation, with imperceptible alteration of the geometry of the strengthened element.

*Corresponding author

Keywords: Torsional strengthening, near surface mounted technique (NSM), carbon fibre reinforced polymer (CFRP)

1. INTRODUCTION AND BACKGROUND

Thin walled reinforced concrete (RC) structures are extensively used in bridge construction as main structural elements. A large number of these aging infrastructure in Europe and across the world is now requiring rehabilitation and strengthening interventions due to degradation, increased traffic loads, upgrades in code requirements and/or deficient constructions. This results in the need of sound maintenance strategies and effective strengthening techniques to ensure safe and functional usage of the structure. For instance, in some of these structures, such as caisson type RC bridges, the increase of their torsional stiffness and strength is mandatory. To the best of the authors knowledge, however, no comprehensive research has been carried out to develop an efficient torsional strengthening solution for tubular type thin walled RC structures and current solutions only rely on complex conventional methods, including: member enlargement, span shortening, application of shotcrete, steel encasing, post tensioning, and external steel plate bonding [1], [2], [3], [4]. All of these traditional methods increase significantly the dead weight of the strengthened structures, while FRP-based strengthening techniques, like the externally bonded reinforcement (EBR) and near surface mounted (NSM) techniques, result in minimal increase in the dead weight of the strengthened structure due to their relatively low specific mass, high stiffness and tensile strength.

Research on torsional strengthening is quite limited in comparison with shear and flexural strengthening and it is only limited to the use of EBR-FRP [5], [6], [7], [8], [9], [10], [11], [12], [13] and [14]. This previous research has explored the influence on the torsional strengthening effectiveness of the following main parameters: FRP strengthening ratio,

number of the strengthened sides of the member (four- and three-sides), strengthening configuration (full wrapping versus discrete strips), interaction between flexure and shear strengthening. The strengthening effectiveness of an EBR-FRP system can be limited by various factors but the bond between the FRP and the concrete substrate is the main governing parameter and is responsible for the majority of premature failures [5]. This has stimulated the development of the NSM technique, which comprises the installation of FRP laminates/bars into thin grooves cut in the concrete cover of the existing structure. The higher surface bond and confinement provided by the surrounding concrete to the NSM-FRP systems increase the strengthening effectiveness of this technique [15], [16], [17]. For the shear strengthening of RC beams, NSM has been demonstrated to be more effective than EBR [19].Although only one investigation was found [18] on torsional strengthening of solid RC elements using NSM FRP, evidence suggests that the use of NSM reinforcement can offer important advantages also for tubular thin walled type RC elements.

A new test setup was designed to ensure that pure torsional actions are developed in the tested specimens to assess the strengthening performance of the NSM technique. The experimental program also aims to obtain information about the influence of the longitudinal and transverse strengthening ratios on the NSM strengthening performance for this type of structures. The experimental program is described in detail, and the relevant results are presented and analysed.

2. PRELIMINARY NUMERICAL ANALYSIS

Due to the innovative character of the experimental program, preparation and development of the test setup and specimens were assisted by numerical simulations using a software based on the finite element method (FEMIX V4.0 [20]). The performance of the constitutive model that was adopted to simulate the nonlinear

behaviour of constituent materials of the RC structures to be investigated was assessed against previous work by Al-Mahaidi and Hii [7] (Fig. 1a). The numerical torsional moment *vs.* angle of rotation is compared with the experimental behaviour in Fig. 1b. The model is capable of simulating with excellent predictive performance the experimental response up to 92% of the ultimate torsional moment recorded experimentally, where the simulation halted due to lack of convergence. Once the model was validated, different strengthening configurations with CFRP laminates were numerically investigated for the proposed RC tubular type beams for guiding the preparation of the experimental work. More details on these numerical simulations are available elsewhere [21], covering the parametric studies for assessing the influence of longitudinal and transverse reinforcement ratios, concrete strength class, strengthening configurations, modulus of elasticity of CFRP, E_f, and use of passive and pre-stressed CFRP reinforcements. As expected, concrete strength highly influenced the torsional cracking moment. All the proposed strengthening configurations improved the ultimate torsional moment carrying capacity, and, by increasing E_f, the yield initiation of longitudinal and transverse reinforcements was delayed.

3. EXPERIMENTAL PROGRAM

3.1. Specimens

The experimental programme consists of six thin walled tubular RC beams with the sectional details shown in Fig. 2. The total length of each beam is 1900 mm, while the effective torsional study area is the central 1000 mm. Additional stirrups are provided at both ends for 450 mm length, to limit damage in these zones due to the development of local high gradient stresses as a result of the loading and clamping conditions in these regions. Eight 10 mm bars form the longitudinal reinforcement, and four-legged stirrups

are provided according to the layout presented in Fig. 2. Two reference beams of C35/45 strength class are prepared, one with one stirrup and the other with four stirrups in the testing region. All four strengthened beams are cast with C35/45 concrete strength class and include four stirrups in the testing zone. Each steel stirrup composing the transverse reinforcement comprises eight legs with two legs on each wall of the beam's cross section.

3.2. Strengthening technique and arrangements

The adopted strengthening configurations are based on the results of the FE analysis and are illustrated in Fig. 3. Four strengthening configurations were adopted by changing the longitudinal and transverse CFRP strengthening ratios. The longitudinal and transverse reinforcement ratios are calculated according to equation (1) and equation (2), respectively, including the existing steel bars and the CFRP strengthening systems converted to equivalent steel reinforcement. Thereby the concept of equivalent reinforcement ratio, $\rho_{l,eq}$ for the longitudinal reinforcement ratio and $\rho_{w,eq}$ for the transverse reinforcement ratio are used:

$$\rho_{l,eq} = \frac{A_{sl}}{\left(bd_s - b_h d_h\right)} + \left[\frac{A_f E_f}{E_s}\frac{1}{\left(bd_f - b_h d_h\right)}\right] \tag{1}$$

$$\rho_{w,eq} = \frac{A_{sw}}{\left(b_w s_w\right)} + \left[\frac{A_f E_f}{E_s}\frac{1}{\left(bs_f\right)}\right] \tag{2}$$

where A_{sl}, b and d_s are, respectively, the cross sectional area, breadth and the internal arm of the existing longitudinal steel bars; A_f and d_f are the cross sectional area and the lever arm of the internal longitudinal CFRP E_s; and E_f are the modulus of elasticity of the steel and CFRP; b_w is the width of web (100 mm); b_h and d_h are the breadth and depth

of the hollow section; A_{sw} and s_w are the cross sectional area and the spacing of the transverse reinforcement (Fig. 2a). The values of these variables are indicated in Table 1. The reference beams are identified by the general acronym of *Ref_bS*, with the following meaning for the characters: *Ref* represents a reference beam; *b* identifies the number of steel stirrups in the central study zone (1000 mm). The general acronym for the strengthened beams is *S_LyTz*, where S represents a strengthened beam, *Ly* is the number (*y*) of CFRP laminates in the longitudinal direction (parallel to the Y axis – longitudinal reinforcement); *Tz* is the number (*z*) of CFRP laminates in the transversal direction (parallel to the Z axis – transverse reinforcement), Fig. 2 and Fig. 3.

For assessing the influence of the existing percentage of steel stirrups in the monitored zone of the beam, one of the reference beams includes only one stirrup in this zone (Ref_1S), while the other reference beam is reinforced with 4 steel stirrups (Ref_4S). Two batches of CFRP laminates are used for strengthening, where beams S_L2S5, S_L2S10 and S_L4S5 are strengthened with the CFRP laminates of the first batch, while S_L4S10 beam is strengthened with the CFRP laminates of the second batch.

During strengthening, the longitudinal CFRP laminates are placed deeper (first) and then the transverse CFRP laminates. Hence, the grooves for the longitudinal CFRP laminates are executed with a depth of 22 mm, while those for the transverse laminates are 12 mm deep. Epoxy 220 resin and CFRP laminates of 10 mm × 1.4 mm cross section from Clever reinforcement Iberica company are used for all the beams. The strengthening involved the following steps:

- Slits of about 5 mm width are opened at the predefined locations using cutting machines;
- The slits are cleaned with high air pressure to remove the dust and to ensure proper bonding between epoxy and concrete substrate;

- CFRP laminates are cleaned with acetone and then the strain gauges are bonded in the pre-established locations;
- The two components of epoxy are mixed in 1:4 ratio according to the specifications and applied inside the slits and on the two larger surfaces of the CFRP laminates;
- CFRP laminates are introduced inside the slits and the excess epoxy is removed. The adhesive is let to cure for a week.

Images of beam S2_L2S10 before and after strengthening are shown in Fig. 4.

3.3. Test setup

The torsional test setup to perform the experimental work is shown in Fig. 5a. It consists of a fixed and a loading end to ensure, as much as possible, clamping support and pure torsional loading conditions. The fixed end of the beam involves steel profiles and a hydraulic jack to secure and avoid any transversal translations or rotations taking place during the tests. In the front end, the beam rests on a pinned support and a circular arc bearing (CAB), which allows the free rotation of the beam at an arc radius of 350 mm from the centre of the beam's cross section, to avoid any additional eccentric forces during the tests. The CAB rests on rollers allowing axial deformation of the beam in Y-direction (Fig. 5a). The direction and rotation of the CAB and rollers are shown in Fig. 5b and 5c. The load is applied through a L type steel profile, part of which is inside the hollow section of the beam up to a length of 300 mm. The other part of this steel loading beam is connected to a load cell at 750 mm from the centre of the beam through multiple hinges, to allow the rotation of the steel loading section with as much minimum friction as possible. Two steel jackets of 52 mm wide, separated at 250 mm are fastened in the loading end of the beam in the over reinforced region to ensure the applied moment is

transferred to the central study area. The tests are performed under displacement control at a displacement rate of 20 $\mu m/s$, with an internal LVDT controlling the actuator.

The torsional angle of rotation is measured in a section at a distance of 200 mm (section Y in Fig. 2b) from the front face of the beam. The coordinates of LVDT's locations are shown in Table 2 by adopting the reference system shown in Fig. 5a. To measure the axial deformation of the beams, LVDT's are placed on the two end sections of the beam, as shown in Fig 5a, 5b and Fig. 8b. Dial gauges are attached to the right and left face extremities of the beam at the fixed end to measure translations (Fig. 2b). Four strain gauges are attached to the steel reinforcement in the central section of the beam (Y=850 mm), two on longitudinal bars and two on transverse bars (on top and left face) as shown in Fig. 2b and Fig. 8b. Four strain gauges are also installed on the CFRP laminates, being as close as possible to the central section of the beam, as illustrated in Fig. 8a. 2D Digital image correlation (DIC) is performed on the left face to measure the concrete strain field during the loading process, but the analysis of this information will be discussed in a future publication due to the extensive obtained data.

4. RESULTS

4.1. Material properties

Concrete cylinders are cast along with the beams to evaluate the average concrete compressive strength, f_{cm}, and modulus of elasticity, E_{cm}, at 28 days. Three and five cylinders are tested to determine the E_{cm} and f_{cm}, respectively, according to standard recommendations [22]. Each cylinder has a diameter of 150 mm and an average height of 300 mm. For the E_{cm} and f_{cm}, values of 34.53 GPa (3.5%) and 31.80 MPa (2.8%) were obtained, respectively (the values in parenthesis are the coefficients of variation). Five samples of the steel bars of 8 mm and 10 mm diameter are tested to determine the

average values of the modulus of elasticity E_{sm}, yield stress f_{ym}, and tensile strength f_{um}, according to the standard EN 10002-1 [23] and the values are presented in Table 3.

The tensile properties of the CFK 150/2000 S&P laminates are characterized by uniaxial tensile tests carried out according to ISO 527-5 with 3 samples [24]. The average elasticity modulus, E_{fm}, and tensile strength, f_{fu}, for the two batches in the experimental program are: 1st batch - E_{fm} = 205.04 GPa (1.2%), f_{fu} = 2346 MPa (5.6%); 2nd batch - E_{fm} = 199.83 GPa (1.4%), f_{fu} = 1982 MPa (3.3%). S&P Resin 220 epoxy adhesive is used to bond the CFRP laminates to the concrete substrate. The instantaneous and long term tensile behaviour of this adhesive was investigated by Costa and Barros [25]. At 3 days, the elasticity modulus ($E_{0.5-2.5\%}$) had attained a stabilized value, the tensile strength and the $E_{0.5-2.5\%}$, determined according to the ISO 527-2 recommendations [26], was about 20 MPa and 7 GPa, respectively.

4.2. Beams

The torsional angle of rotation *vs*. torsional moment of S_L2S10 is represented in Fig. 6a, and is used to introduce the variables, whose results will be presented and commented. The experimental torsional response of this representative beam can be decomposed in to the following main phases:

1) linear response up to the formation of visible cracks in the external faces of the beam ($\theta_{t,cr}$, $M_{t,cr}$). The stiffness of this phase is characterized by the inclination of the line connecting the test initiation and the point corresponding to ($\theta_{t,cr}$, $M_{t,cr}$), $k_{t,lin} = M_{t,cr} / \theta_{t,cr}$. Analysing in depth the shape of θ_t - M_t in this phase, it is verified a certain extent of nonlinearity, which was caused by the formation of few cracks in the loading branch of the beams due to the high tensile stresses developed in the zone;

2) A crack propagation phase where loading-unloading cycles have occurred with the increase of the torsional angle. The amplitude of these cycles has decreased during the loading process (performed under displacement control) up to the stage where crack propagation is stabilized (point C) and no more relevant cracks are formed. Deep analysis of the obtained results has pointed out that the crack stabilization process has almost coincided with the yield initiation of the steel reinforcement (longitudinal and transverse steel yielding simultaneously in Ref_4S beam and alternatively in strengthened beams). Therefore, to simplify the analysis without compromising the reliability on the relevant conclusions, herein it is assumed that crack stabilization process coincided with the occurrence of first yield initiation of the steel reinforcement. This cracking phase (identified by the *cp* subscript) can be decomposed in two sub-stages, one from crack initiation up to the first drop in the torsional moment capacity, identified by the point *B*, and the second from point *B* to *C*. The last point C represents the yield initiation of the steel reinforcement, identified by $\theta_{t,syi}$ and $M_{t,syi}$. These first and second sub-stages are characterized by the propagation of micro- and macro-cracks, therefore the respective subscripts, *μcr* and *Mcr*, are used for their identification. These micro- and macro-crack propagation sub-stages are identified by the following respective increment of torsional angle and torsional moment: $\Delta\theta_{t,\mu cr}$, $\Delta M_{t,\mu cr}$; $\Delta\theta_{t,Mcr}$, $\Delta M_{t,Mcr}$. The macro-crack propagation sub-stage is also identified by the stiffness, $k_{t,Mcr} = \Delta M_{t,Mcr} \big/ \Delta\theta_{t,Mcr}$, which is the inclination of a line that best fits the experimental response of this sub-stage. In the context of an analytical model (an ongoing research), the θ_t - M_t response in the cracking stage is modelled by segment AC, where point A is determined by the intersection of lines defined by $k_{t,lin}$ and $k_{t,Mcr}$;

3) The third phase covers the stage from yield initiation in the steel reinforcement ($\theta_{t,syi}$, $M_{t,syi}$) up to the peak load ($\theta_{t,p}$, $M_{t,p}$). The CFRP strengthening systems are mainly activated in this phase by increasing the stiffness and the torsional capacity. The initial stiffness of this phase, $k_{t,syi}$, is the initial tangent to θ_t - M_t response. This initial response is characterized by an almost constant stiffness that ends at a stage identified by a red marker in the curve, which is followed by a gradual decrease of stiffness due to the yielding of more steel bars, as well as debonding between reinforcements (and also CFRP systems in case of strengthened beams) and surrounding concrete. The increment of torsional moment and torsional angle in this elasto-plastic cracked stage is represented by $\Delta M_{t,syp}$ and $\Delta\theta_{t,syp}$.

The θ_t - M_t of all the tested beams are presented in Fig. 6b, and the relevant results are included in Table 4, 5 and 6. Considering the same concrete strength class which was adopted for all the experimental programme, $k_{t,lin}$ was expected to be the same for the tested beams. However, some differences were registered, which can be justified by the susceptibility of $k_{t,lin}$ at the precise capture of point ($\theta_{t,cr}$, $M_{t,cr}$), whose determination has the expected uncertainty on the detection of the crack initiation. This difficulty is amplified due to the probability of similar crack occurance on all four external faces.

Apart S_L2S5 beam, the other strengthening configurations have provided an increase on the $M_{t,cr}$, while increase of $\theta_{t,cr}$ was only registered in the two strengthening configurations with four longitudinal CFRP laminates (S_L4S5 and S_L4S10). Regarding (θ_t , M_t) of point A of cracking angle $\theta_{t,A}$ and cracking moment $M_{t,A}$, average values of, respectively, 0.73 degrees and 47.15 kN·m were obtained considering

all the beams, with much higher COV for the $\theta_{t,A}$ (38%) than for $M_{t,A}$ (13%) due to its higher susceptibility to $k_{t,lin}$. In any case, a tendency for the increase of $\theta_{t,A}$ with the percentage of longitudinal CFRP laminates is evident (almost the double), while the increase of $M_{t,A}$ in the strengthened beams was not so accentuated.

The stiffness at the macro-crack propagation, $k_{t,Mcr}$, has increased in the beams strengthened with 2 longitudinal CFRP laminates and has decreased in the beams strengthened with 4 longitudinal CFRP laminates. As the variation level was very small, it is possible to conclude that for the adopted strengthened configurations the $k_{t,Mcr}$ is almost the same as the reference beam.

Regarding the torsional moment at yield initiation of the steel reinforcement, $M_{t,syi}$, transverse CFRP laminates are more effective than longitudinal ones. In terms of torsional angle at yield initiation, $\theta_{t,syi}$, it has increased only in the beams with highest percentage of longitudinal CFRP laminates, but limited to 7%. The adopted strengthening configurations have not changed significantly the stiffness at steel yield initiation, $k_{t,syi}$, with respect to the reference beam. An average value of 6.97 kN·m/deg. with COV of 11% is registered for $k_{t,syi}$ in all the tested beams.

Regarding the torsional moment at peak load ($M_{t,p}$) the increase provided by the adopted strengthened configurations has varied between 38% and 46%, with largest increase in beams with highest percentage of transverse CFRP laminates. The adopted strengthened configurations were also very effective in increasing the torsional angle at peak load ($\theta_{t,p}$), which can be referred as a ductility indicator. This increase ranged between 53% and

76%, where the minimum value was registered in the beam with both smallest longitudinal and transverse strengthening ratios (S_L2S5). In the other three strengthened beams $\theta_{t,p}$ was very similar, so no clear conclusions can be extracted for the dominance of longitudinal versus transverse CFRP laminates on the torsional deformability of this type of RC beams.

Fig. 7a compares the θ_t - M_t response of two reference RC beams, the Ref_1S with only one steel stirrup in the monitored span, while the Ref_4S has four steel stirrups in this span. It is verified that by increasing the reinforcement ratio of existing steel stirrups (ρ_{sw}) from 0.050% to 0.502%, the torsional moment and torsional angle at crack initiation and at peak load have increased significantly. This indicates that the lower is the ρ_{sw} the larger is the potential of the CFRP laminates in increasing the torsional resistance and deformability of this type of RC structures, a subject that is part of the ongoing research. This is in alignment with the interference of existing steel stirrups and NSM CFRP laminates applied for increasing the shear capacity of RC beams, where available experimental research [27] and analytical models [28] demonstrate that the strengthening effectiveness decreases with the increase of existing percentage of steel stirrups.

Fig. 7b shows the relationship between the applied torsional moment *vs* the axial deformability of the Ref_4S beam, where the axial deformability was recorded in the clamping and loading extremities by the LVDT's disposed according to the schematic representation shown in Fig. 8b. For the axial deformation positive values are assumed for elongation. It is verified that the LVDTs disposed at the top and bottom flanges of the extremity at the loaded zone have recorded almost equal displacement of elongation up to the torsional strength of the beam. The LVDT disposed at the top flange of the extremity at the clamping zone has also registered an elongation of the beam, but, as

expected, of much smaller value. The elongation and corresponding beam's axial deformation at torsional strength was 6.69 mm and 3.52‰ in the Ref_4S beam. The corresponding average values of 10.97 mm and 5.77‰ for the strengthened beams, with a COV of 11.2%, indicate that all the strengthened beams have experienced similar elongation, of about double the reference beam. The elongation is mainly caused by the axial component of the opening registered in the cracks formed during the loading process of the beam. The strengthened beams presented larger axial deformation than the reference beam, mainly due to the higher torsional deformability at failure.

4.3. Strains in the steel reinforcements and CFRP laminates

The relationships between strain in the strain gauges (SG) applied in the steel reinforcements and torsional angle for the reference and strengthened beams are presented in Fig. 8a and Fig. 9. The vertical dashed and dotted lines indicate the yielding strain in the longitudinal and the transverse steel reinforcements at 2675 $\mu\varepsilon$ and 3376 $\mu\varepsilon$, respectively. The location and designation of the adopted SG's are indicated in Fig. 8b, while their precise co-ordinates are presented in Table 7 according to the co-ordinate system adopted in Fig. 5a. The values recorded in some SG are not presented due to deficient functioning of these SG. The letters L and T in the adopted acronym stand for representing the strain gauges applied in the Longitudinal and Transverse reinforcement/CFRP-laminate, while S and F represent Steel and CFRP-laminate. For instance, SG_LS1 is the strain gauge number 1 (applied on the top face of the beam, Fig. 8b) installed on a longitudinal steel bar; SG_TF2 is the strain gauge number 2 (applied on a lateral face of the beam, Fig. 8b) installed on a transverse CFRP laminate.

The values of steel and CFRP strains at $\theta_{t,syi}$, $\theta_{t,p}$ and $\theta_{t,u}$ (when the test has ended) are indicated in Tables 8 and 9. In Fig. 8a and Fig. 9 horizontal lines are included

corresponding to $\theta_{t,Mcr}$, $\theta_{t,syi}$, and $\theta_{t,p}$. As expected, Fig. 8a shows that up to $\theta_{t,Mcr}$ the steel strains are very small due to the almost inactivation of the reinforcement. Abrupt increase in the strains occurred between $\theta_{t,Mcr}$ and $\theta_{t,syi}$, i.e., during the cracking propagation stage. This also happens in the strengthened beams, not only in the steel reinforcement, but also in the CFRP laminates. However, in the Ref_4S beam two of the three SG have presented an abrupt increase of negative strain values (compression), while in the strengthened beams, as expected, the abrupt increase of strain was always positive (tensile strain) in both the steel reinforcement and the CFRP laminates. The abrupt increase of negative strain in the Ref_4S might be justified by a local phenomenon related to the relative distance between the SG (where these values were recorded) and the closest crack. If a dominant sliding happens over opening at a crack crossed by the reinforcement, a local curvature can be developed in the reinforcement at the cracked section. If a SG is localized in this zone, it can record negative strain values.

After the abrupt increase in the strains recorded in the steel reinforcements, Ref_4S presented a gradient of strains higher than the one registered in the SG applied in the strengthened beams (apart the exception of the strain recorded in the SG_TS1 of S_L4S10 beam). This can be justified by the contribution of the CFRP laminates crossing the cracks by promoting the development of higher number of cracks, but of smaller crack width. No clear tendency is detected in the type of reinforcement (longitudinal or transverse) where the maximum strains have occurred, since this depends significantly on the relative position between the SG and the closest crack.

Regarding the strains in the CFRP laminates (Fig. 9), the maximum strains have, in general, occurred in the SG_TF1, i.e. in the transverse CFRP laminate located on the top face of the strengthened beams (Fig. 8b). Like the SG installed in the steel bars, the gradient of strain in the CFRP laminates is also quite dependent of the position of the SG

regarding the closest crack. Fig. 9 and Table 9 show that the maximum strain in the CFRP laminates at $\theta_{t,p}$ was 11.05‰, which corresponds to 88.50% of the ultimate tensile strain of these laminates.

The premature delamination of CFRP in corners due to bond failure or stress concentration, usually experienced in EBR technique for torsion [5], was not observed in any of the adopted NSM strengthening configurations.

4.4. Influence of CFRP strengthening ratios on the torsional performance of the tested beams

In order to assess the influence of the longitudinal CFRP strengthening ratio on torsional behaviour of the strengthened beams, the torsional angle vs torsional moment (θ_t - M_t) of beams S_L2S5 and S_L4S5 are compared in Fig. 11a and for S_L2S10 and S_L4S10 are compared in Fig. 11b. For the adopted flexural strengthening configurations, it is verified that increasing ρ_{fl} from 0.096 to 0.192 (Table 1) had marginal contribution in terms of torsional capacity and deformability. The θ_t - M_t of the S_L2S5 and S_L2S10 beams are compared in Fig. 10c, while this comparison for the S_L4S5 and S_L4S10 are shown in Fig. 10d, in order to assess the influence of the transverse CFRP strengthening ratio on torsional behaviour of the tested strengthened beams. For the adopted transverse strengthening configurations it is verified that increasing ρ_{fw} from 0.071 to 0.141 (Table 1) had similar increase in both groups of beams in terms of torsional capacity, but limited to 4.5%. This increase is mainly due to the moment at macro-crack initiation ($M_{t,Mcr}$) that increased 12.65%. The stiffness for torsional deformation above $\theta_{t,Mcr}$ was marginally affected by the adopted ρ_{fw}. In terms of maximum torsional deformation, an

increase is observed in the first group, while it is decreased in the second group. However, it should be mentioned that the test of S_L4S10 beam was ended prematurely to avoid damage in some of the LVDTs. Therefore, it is expectable that ultimate torsional deformation would also have increased with increase of ρ_{fw}.

4.5. Crack spacing and orientation, and failure modes

The average crack spacing (s_{rm}) and average crack orientation (α_{crm}) is determined according to the strategy described in Fig. 12a and equations (3) and (4). s_{rm} is calculated as an average spacing of the cracks crossing the four edges of the beam in the monitored span, according to equation (3), where s_i (i=1 to n) is crack spacing and n is number of cracks. α_{crm} is evaluated as an average crack inclination along the four faces of the beam using equation (4). Each inclination is determined by an imaginary line connecting the cracks from one edge to the other on each face as shown in Fig. 12b. The values of s_{rm} and α_{crm} for the tested beams are presented in Table 10, while Fig. 13 and Fig. 14 represent the crack pattern at the failure of the reference and strengthened beams, respectively.

$$s_{rm} = \frac{s_1 + s_2 + s_3 + ... + s_n}{n} \tag{3}$$

$$\alpha_{crm} = \frac{\tan^{-1}\left(\frac{y}{x_1}\right) + \tan^{-1}\left(\frac{y}{x_2}\right) + \tan^{-1}\left(\frac{y}{x_3}\right) + ... + \tan^{-1}\left(\frac{y}{x_n}\right)}{n} \tag{4}$$

In the reference beams (Fig. 13) the s_{rm} of Ref_4S (200 mm) is less than half the s_{rm} of Ref_1S (412mm), evidencing the high influence of the existing percentage of steel stirrups, with consequent impact on the torsional performance as already discussed. However, the α_{crm} was equal in these two beams (50 degrees).

Regarding the strengthened beams (Fig. 14) it is verified that the transverse CFRP laminates are more effective than the longitudinal CFRP laminates in decreasing the s_{rm}. In fact, the s_{rm} of the beams reinforced with the highest transverse strengthening ratio (S_L2S10 and S_L4S10 beams) is almost equal, with an average value of 102 mm, whereas the s_{rm} of the beams reinforced with the lowest transverse strengthening ratio (S_L2S5 and S_L4S5 beams) is equal to 133 mm. The α_{crm} in the strengthened beams is almost equal to the one of the reference beams, varying between 49 and 54 degrees.

Ref_1S beam had a brittle concrete failure (Fig. 13a) with the formation of very small number of wider cracks due the existence of only one stirrup in the tested beam's span. However, Ref_4S has failed in a much more ductile behaviour due to the formation of several cracks due to the contribution of four steel stirrups (as seen in Fig. 8a, longitudinal and transverse reinforcements have yielded).

The S_L2S5 and S_L2S10 beams failed by CFRP rupture followed by concrete crushing (with spalling) on the right and top face (Fig. 15, Fig. 16a and Fig. 16b). S_L4S5 beam also failed with CFRP rupture and crushing of concrete but on the left and top surfaces (Fig. 16c). S_L4S10 beam had a premature concrete failure on the top surface between the steel jackets (Fig. 16d). In spite of which beam S_L4S10 presented the maximum torsional capacity. In S_L2S5, S_L2S10 and S_L4S10 beams the rupture of CFRP laminates was confirmed by post-testing inspections.

5. CONCLUSIONS

The current paper assesses experimentally the performance of NSM FRP reinforcement in enhancing the torsional behaviour of thin walled tubular reinforced concrete structures. The key parameters investigated in this study were (a) longitudinal CFRP reinforcement

ratio and (b) transverse CFRP reinforcement ratio. The main conclusions from this study are the following:

- The adopted NSM-CFRP strengthening configurations provided an increase not only in maximum torsional moment, $M_{t,p}$ (between 38% and 46%) but also in $\theta_{t,p}$ (53 % - 76%), $M_{t,cr}$ (2% - 40%), stiffness after crack stabilized stage (43% - 59%) and $M_{t,syi}$ (12% - 34%);
- The conceived test setup is very successful in assessing the performance of torsional tests. Most of the reinforcements both in the longitudinal and transverse directions have yielded, f_{ym}. The CFRP reinforcements have reached strains of 11358 $\mu\varepsilon$ (89% of its tensile capacity) proving their efficacy in torsional applications;
- The contribution of transverse CFRP laminates is more important than that of the longitudinal CFRP laminates in determining overall structural performance, including $M_{t,p}$, $\theta_{t,p}$, s_{rm} and arrest in crack propagation;
- All strengthened beams have undergone elongation (0.53%) due to crack sliding and crack opening. Beams S_L2S5, S_L2S10 and S_L4S5 have failed by CFRP rupture followed by concrete crushing and beam S_L4S10 had premature failure in the over reinforced region;
- Considering the average spiral crack spacing, the CFRP strengthened beams have reduced crack spacing ranging between 33% and 49%, confirming that the NSM CFRP is very effective in reducing the crack growth and limiting the crack width.

ACKNOWLEDGMENTS

The first author would like to thank the Marie Curie Initial Training Network "Endure" MC-ITN-2013-607851, European Network for Durable Reinforcement and Rehabilitation Solutions, for the grant received to perform the research. Also, to the industries CASAIS and CiviTest in helping to execute the experimental work. The support provided by FCT through the PTDC/ECM-EST/1882/2014 project is also acknowledged.

DATA AVAILABILITY STATEMENT

The raw/processed data required to reproduce these findings cannot be shared at this time as the data also forms part of an ongoing study.

REFERENCES

[1] Emmons PH, Vaysburd AM, Thomas J. Strengthening concrete structures, Part I. Concr Int 1998;19:53–8.

[2] Rodriguez M, Park R. 203-Repair-strengthening-reinforced-concrete-buildings.pdf. Earthq Spectra 1991;7:439–59.

[3] Schladitz F, Curbach M. Increase in the Torsional Resistance of Reinforced Concrete Members using Textile Reinforced Concrete (TRC). Concr. Repair, Rehabil. Retrofit. II, 2009, p. 1095–100.

[4] Alkhrdaji BT, Thomas J. Methods of Upgrading Concrete Structures. 2002.

[5] Panchacharam S, Belarbi A. Torsional Behavior of Reinforced Concrete Beams Strengthened with FRP Composites. First FIB Congr. Concr. Struct. 21st Century, Osaka, Japan, Oct. 13-19,2002, 2002, p. 1–11.

[6] Deifalla A, Ghobarah A. Simplified analysis for Torsionaly Strengthened RC Beams Using FRP. Proc. Int. Symp. Bond Behav. FRP Struct. (BBFS 2005), Hong Kong, December 5-7, 2005, 2005.

[7] Hii AKY, Al-Mahaidi R. An experimental and numerical investigation on torsional strengthening of solid and box-section RC beams using CFRP laminates. Compos Struct 2006;75:213–21. doi:10.1016/j.compstruct.2006.04.050.

[8] Jing M, Raongjant W, Li Z. Torsional strengthening of reinforced concrete box beams using carbon fiber reinforced polymer. Compos Struct 2007;78:264–70. doi:10.1016/j.compstruct.2005.10.017.

[9] Al-Mahaidi R, Hii AKY. Bond behaviour of CFRP reinforcement for torsional strengthening of solid and box-section RC beams. Compos Part B Eng 2007;38:720–31. doi:10.1016/j.compositesb.2006.06.018.

[10] Chalioris CE. Behavioural model of FRP strengthened reinforced concrete beams

under torsion. J Compos Constr 2007;11:192–200. doi:10.1061/(ASCE)1090-0268(2007)11:2(192).

[11] Chalioris CE. Torsional strengthening of rectangular and flanged beams using carbon fibre-reinforced-polymers - Experimental study. Constr Build Mater 2008;22:21–9. doi:10.1016/j.conbuildmat.2006.09.003.

[12] Deifalla A, Ghobarah A. Strengthening RC T-Beams Subjected to Combined Torsion and Shear Using FRP Fabrics: Experimental Study. J Compos Constr 2010;14:301–11. doi:10.1061/(ASCE)CC.1943-5614.0000091.

[13] Deifalla A, Awad A, Elgarhy M. Effectiveness of externally bonded CFRP strips for strengthening flanged beams under torsion: An experimental study. Eng Struct 2013;56:2065–75. doi:10.1016/j.engstruct.2013.08.027.

[14] Deifalla A, Hamed M, Saleh A, Ali T. Exploring GFRP bars as reinforcement for rectangular and L-shaped beams subjected to significant torsion: An experimental study. Eng Struct 2013;59:776–86. doi:10.1016/j.engstruct.2013.11.027.

[15] Barros JAO, Fortes AS. Flexural strengthening of concrete beams with CFRP laminates bonded into slits. Cem Concr Compos 2004;27:471–80. doi:10.1016/j.cemconcomp.2004.07.004.

[16] Lorenzis DL, Nanni A. Shear Strengthening of Reinforced Concrete Beams with Near-Surface Mounted Fiber-Reinforced Polymer Rods. ACI Struct J 2001;98(1):60–8.

[17] El-Hacha R, Rizkalla SH. Near-surface-mounted fiber-reinforced polymer reinforcements for flexural strengthening of concrete structures. ACI Struct J 2004;101:717–26. doi:10.14359/13394.

[18] Al-Bayati G, Al-Mahaidi R, Kalfat R. Torsional strengthening of reinforced concrete beams using different configurations of NSM FRP with epoxy resins and

cement-based adhesives. Compos Struct 2017;168:569–81. doi:10.1016/j.compstruct.2016.12.045.

[19] Barros J a O, Dias SJE, Lima JLT. Efficacy of CFRP-based techniques for the flexural and shear strengthening of concrete beams. Cem Concr Compos 2007;29:203–17. doi:10.1016/j.cemconcomp.2006.09.001.

[20] Gouveia AV. Constitutive models for the material nonlinear analysis of concrete structures including time-dependent effects. University of Minho, Guimaraes, Portugal, 2011.

[21] Gowda CC, Barros JAO. Exploring NSM technique for torsional strengthening of tubular type RC structures. 11th fib Int. Symp. Civ. Eng., University of Tokyo, Japan, Aug 29th-31st, 2016: 2016, p. 1–8.

[22] BS EN 12390-3 (2009). Testing hardened concrete. vol. 3. 2009.

[23] ISO 6892-1. Metallic materials — Tensile testing — Part 1: Method of test at room temperature. vol. 2009. 2009.

[24] ISO 527-5. Plastics — Determination of tensile properties - Part 5: Test conditions for unidirectional fibre-reinforced plastic composites. vol. 1. 1997.

[25] Costa IG, Barros JAO. Tensile creep of a structural epoxy adhesive: experimental and analytical characterization. Int J Adhes Adhes 2015;59:115–24. doi:10.1002/pssb.201451168.

[26] ISO527-2. Plastics - Determination of tensile properties - Part 2: Test conditions for moulding and extrusion plastics. 1993.

[27] Dias SJ., Barros JAO. Shear strengthening of RC beams with NSM CFRP laminates: Experimental research and analytical formulation. Compos Struct J 2013;99:477–90. doi:http://dx.doi.org/10.1016/j.compstruct.2012.09.026.

[28] Bianco V, Monti G, Barros JAO. Design formula to evaluate the NSM FRP strips

shear strength contribution to a RC beam. Compos Part B Eng 2014;56:960–71. doi:10.1016/j.compositesb.2013.09.001.

List of Figures

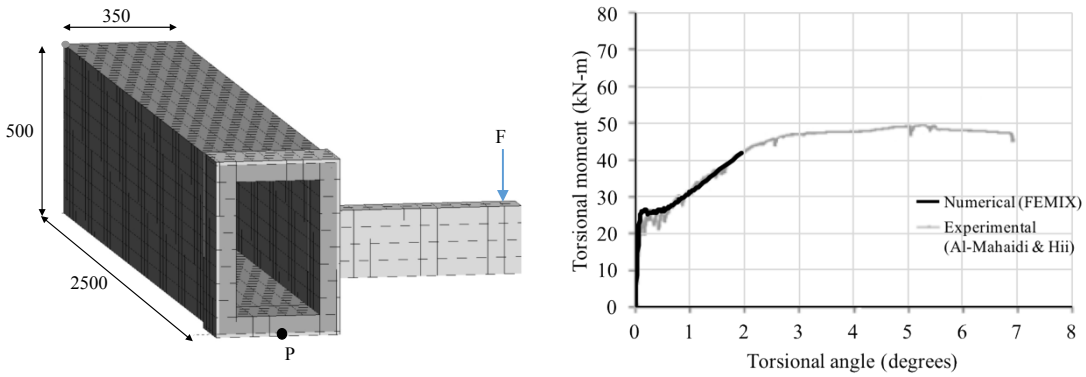

a) b)

Fig. 1 - a) Simulation of experimental beam tested in [7] in FEMIX (dimensions in mm); b) torsional moment – torsional angle of rotation, numerical and experimental

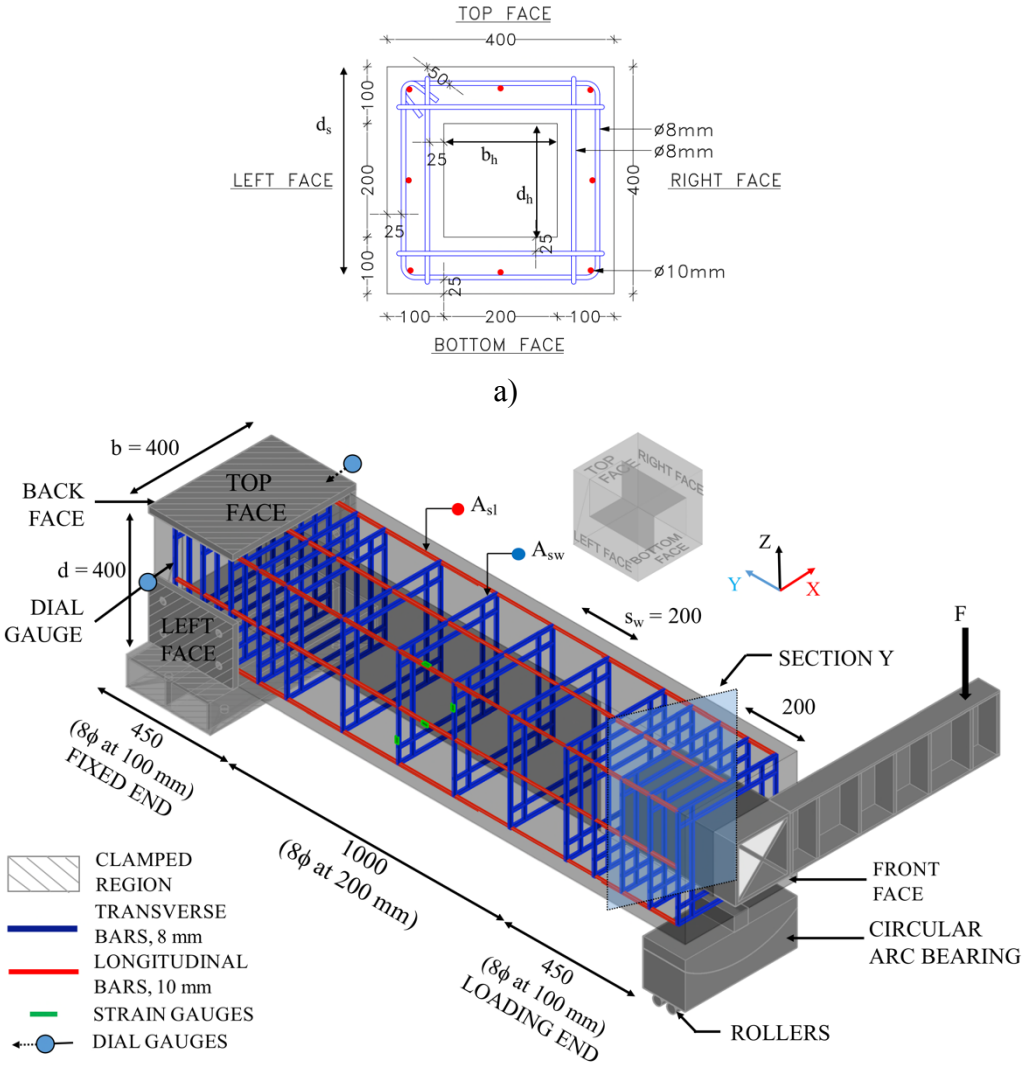

Fig. 2 - Beam details: a) Cross section; b) Longitudinal details (dimensions in mm)

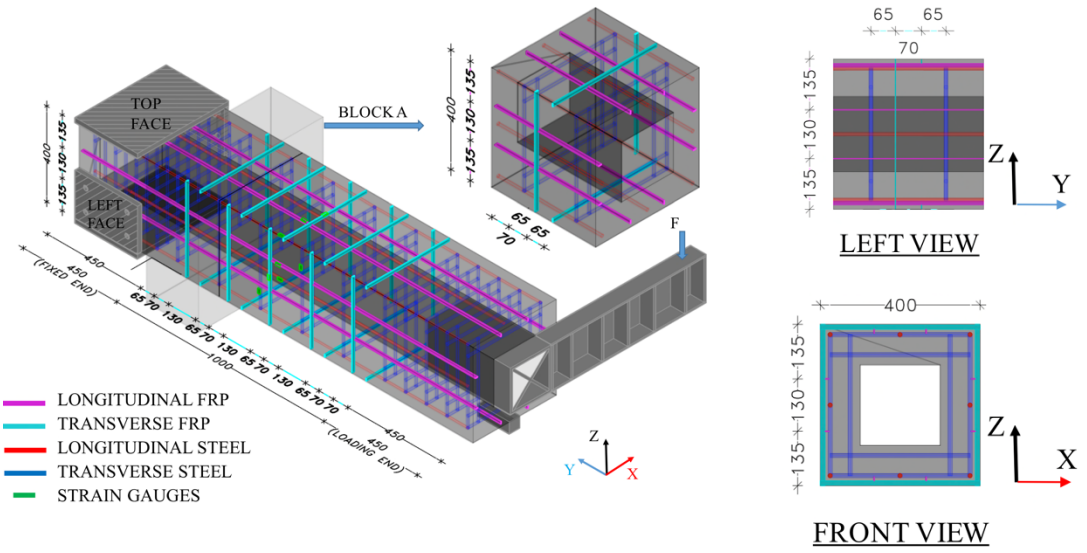
TOP FACE
LEFT FACE
BLOCK A
F
LONGITUDINAL FRP
TRANSVERSE FRP
LONGITUDINAL STEEL
TRANSVERSE STEEL
STRAIN GAUGES
LEFT VIEW
FRONT VIEW

a)

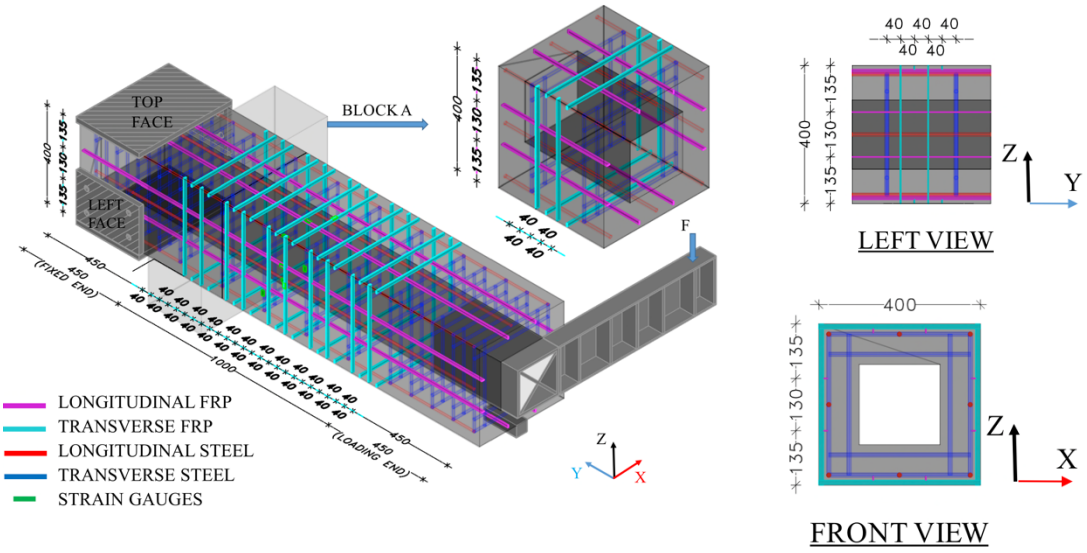
TOP FACE
LEFT FACE
BLOCK A
F
LONGITUDINAL FRP
TRANSVERSE FRP
LONGITUDINAL STEEL
TRANSVERSE STEEL
STRAIN GAUGES
LEFT VIEW
FRONT VIEW

b)

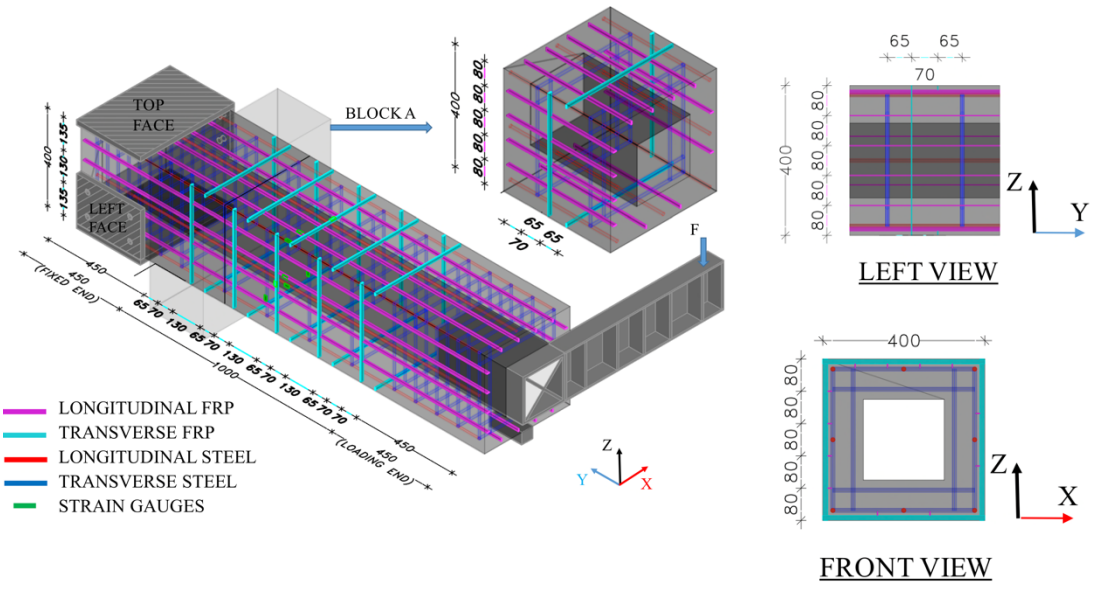
TOP FACE
LEFT FACE
BLOCK A
F
LONGITUDINAL FRP
TRANSVERSE FRP
LONGITUDINAL STEEL
TRANSVERSE STEEL
STRAIN GAUGES
LEFT VIEW
FRONT VIEW

c)

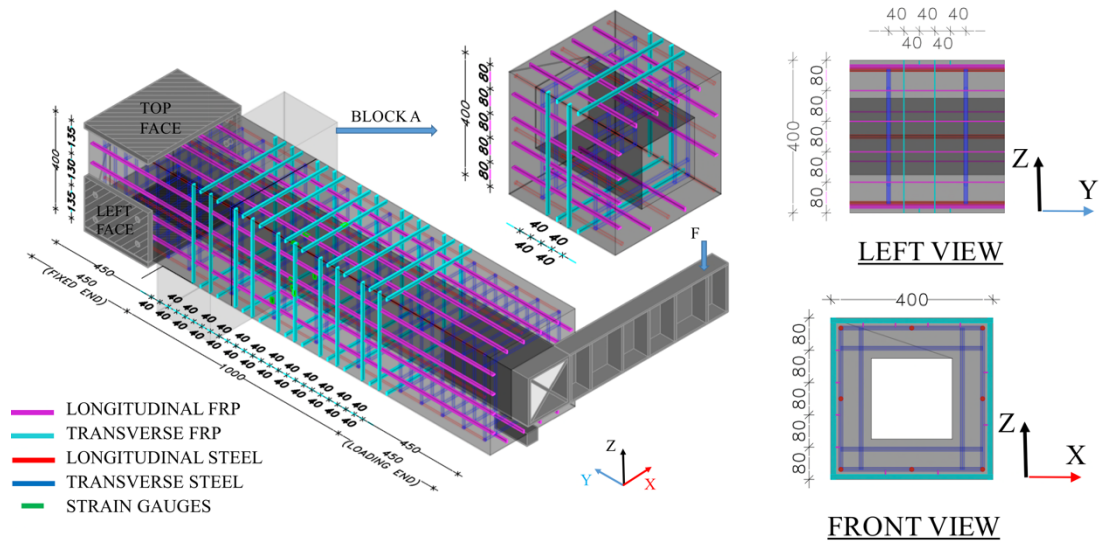

d)

Fig. 3 - Strengthening configurations: a) S1_L2S5; b) S2_L2S10; c) S3_L4S5; and d) S4_L4S10 (dimensions in mm)

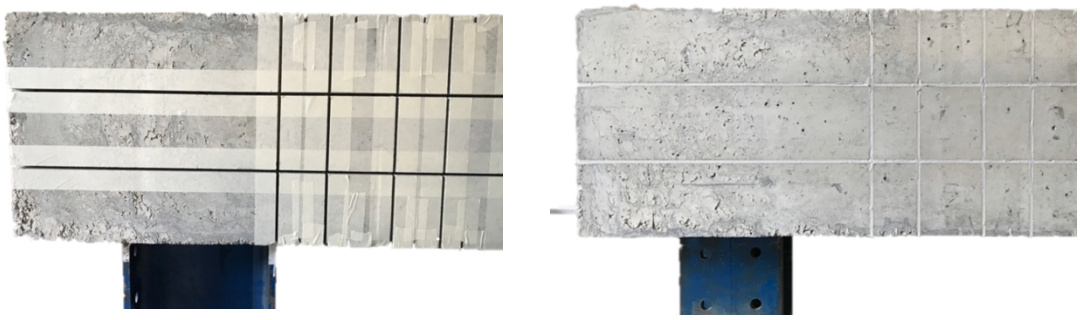

a) b)

Fig. 4 - Strengthening stages of S2_L2S10 beam: a) Localization of the slits; b) appearance after strengthening

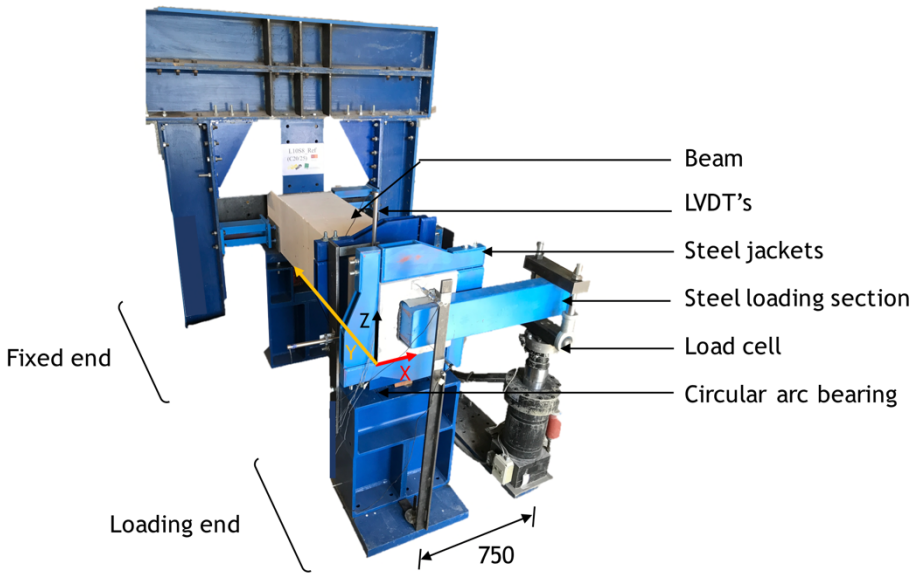

a)

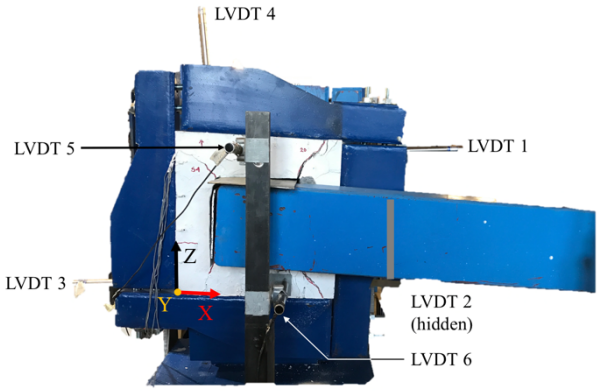

b)

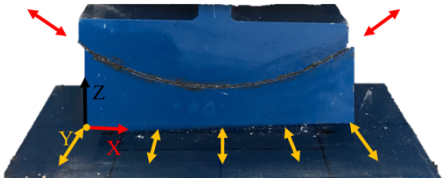

c)

Fig. 5 - a) Test setup; b) LVDT locations; and c) Circular arc bearing

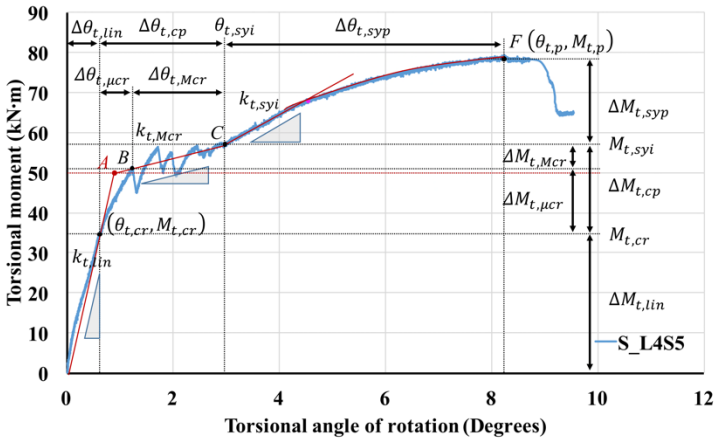

a)

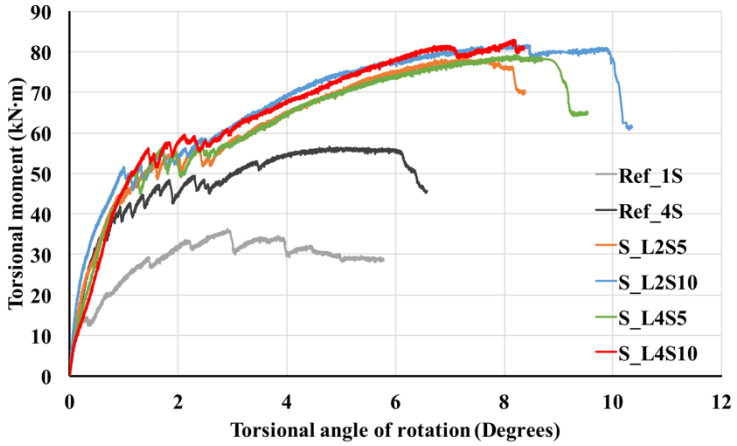

b)

Fig. 6 - Torsional moment vs torsional angle of rotation: a) graphical representation of the notations; b) strengthened beams

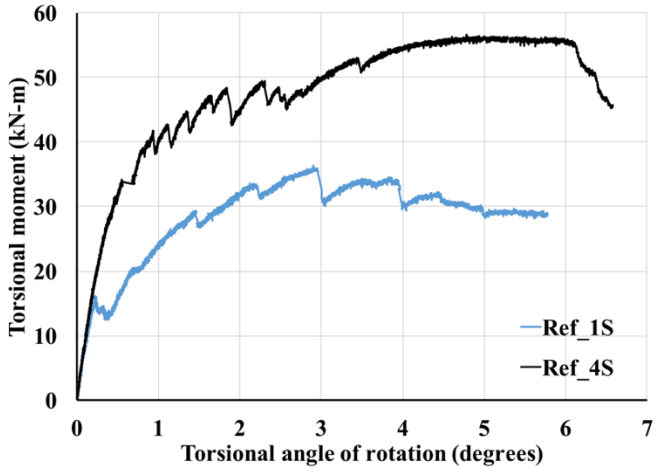

a)

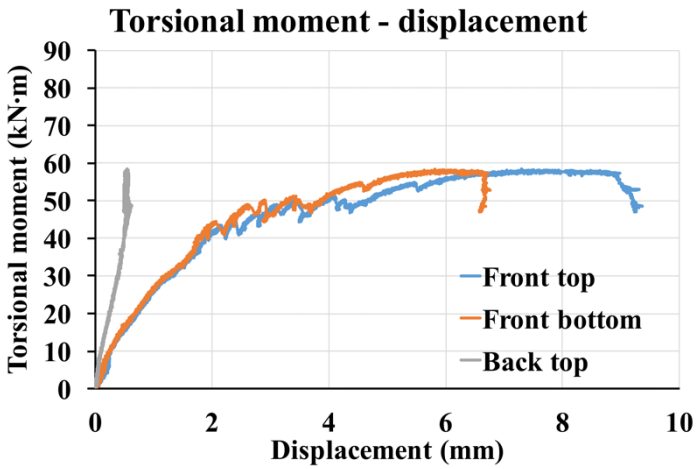

b)

Fig. 7 – Reference beams: a) Torsional moment vs angle of rotation of reference beams; b) torsional moment vs axial deformation of reference beam Ref_4S

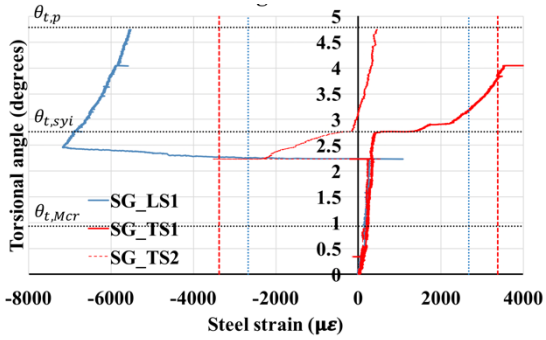

a)

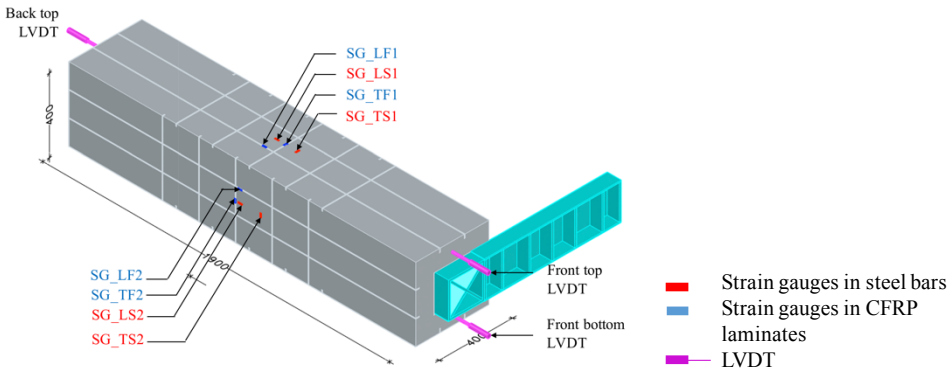

b)

Fig. 8 - Ref_4S: a) Torsional moment vs strain in the steel reinforcements; b) Localization of strain gauges and LVDT's

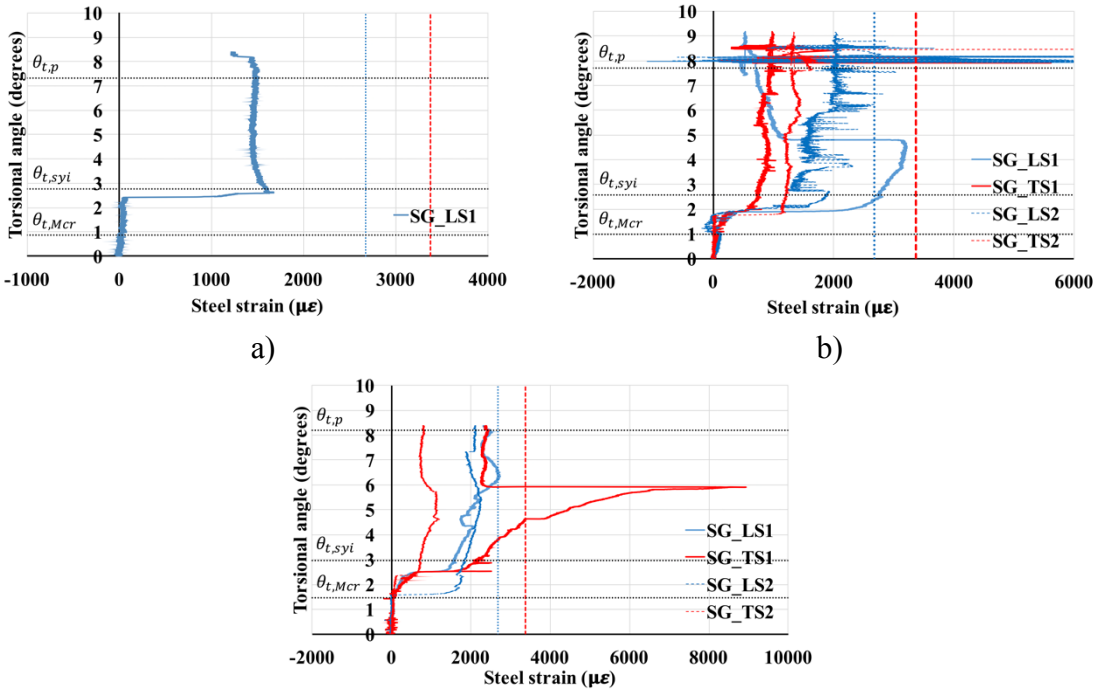

Fig. 9 – Torsional moment vs strains in the steel reinforcements of beams: a) S_L2S5; b) S_L2S10; and c) S_L4S10

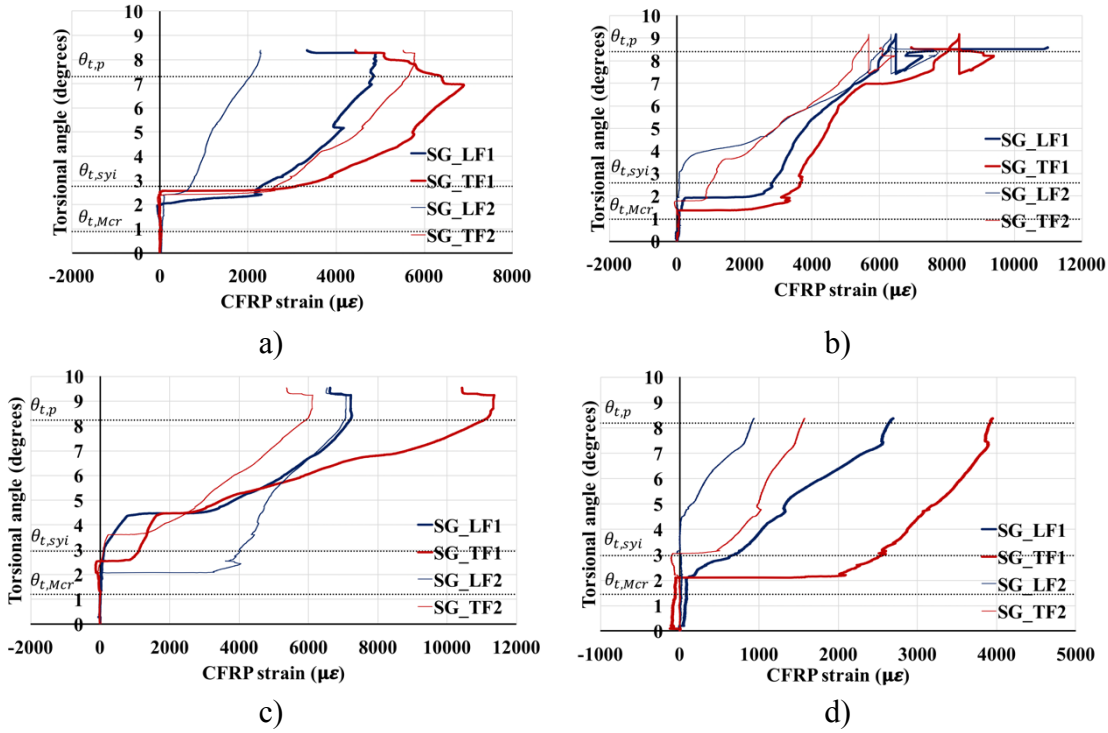

Fig. 10 – Torsional moment vs strains in CFRP laminates of beams: a) S_L2S5; b) S_L2S10; c) S_L4S5; and d) S_L4S10

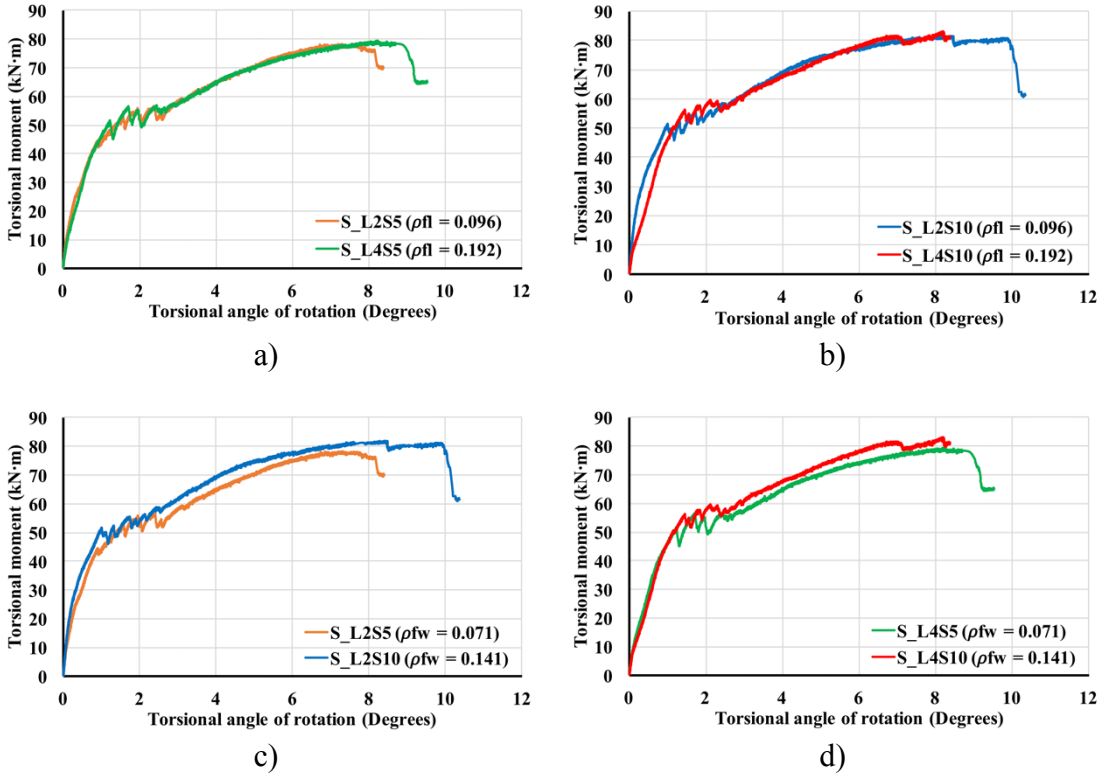

Fig. 11 - Influence of CFRP strengthening ratio of type: a) and b) longitudinal; c) and d) transverse

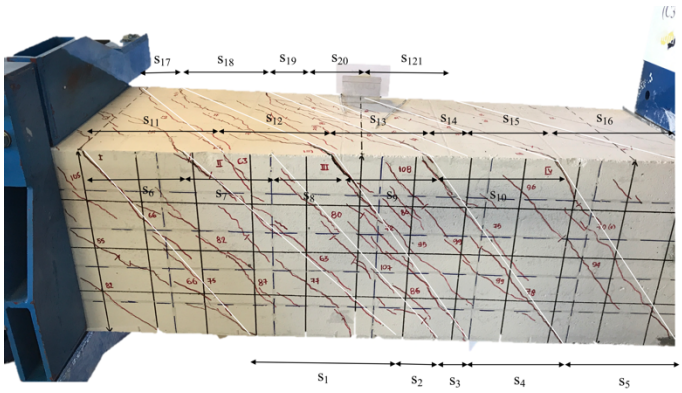

(a)

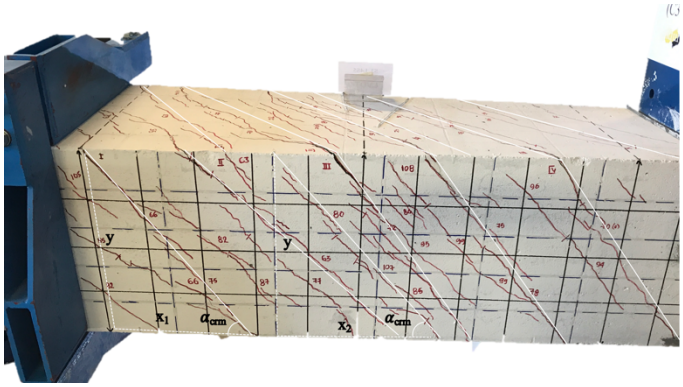

(b)

Fig. 12 – Schematic procedure for determining: a) average crack spacing (s_{rm}); and b) average crack orientation (α_{crm})

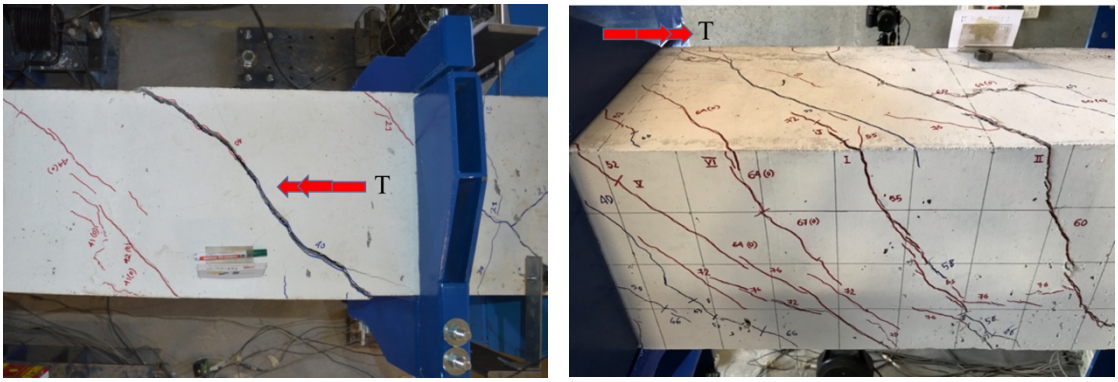

a) b)

Fig. 13 - Crack pattern at failure of beams: a) Ref_1S; and b) Ref_4S

a)

b)

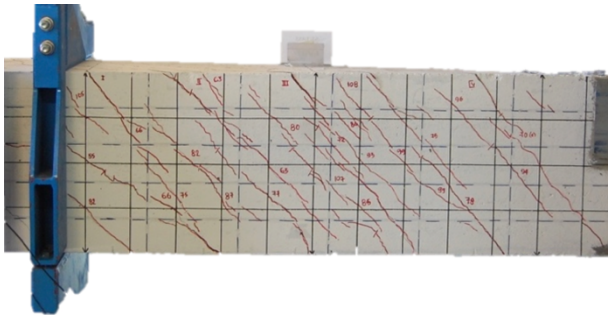

c)

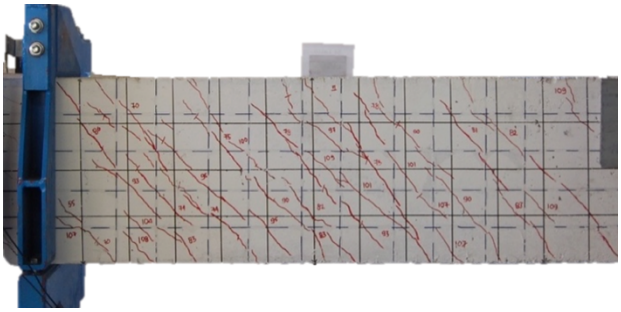

d)

Fig. 14 - Crack pattern in the right face at the failure of the beam: a) S_L2S5; b) S_L2S10; c) S_L4S5; and d) S_L4S10

a) b)

Fig. 15 - CFRP rupture in beams: a) S_L2S5; and b) S_L2S10

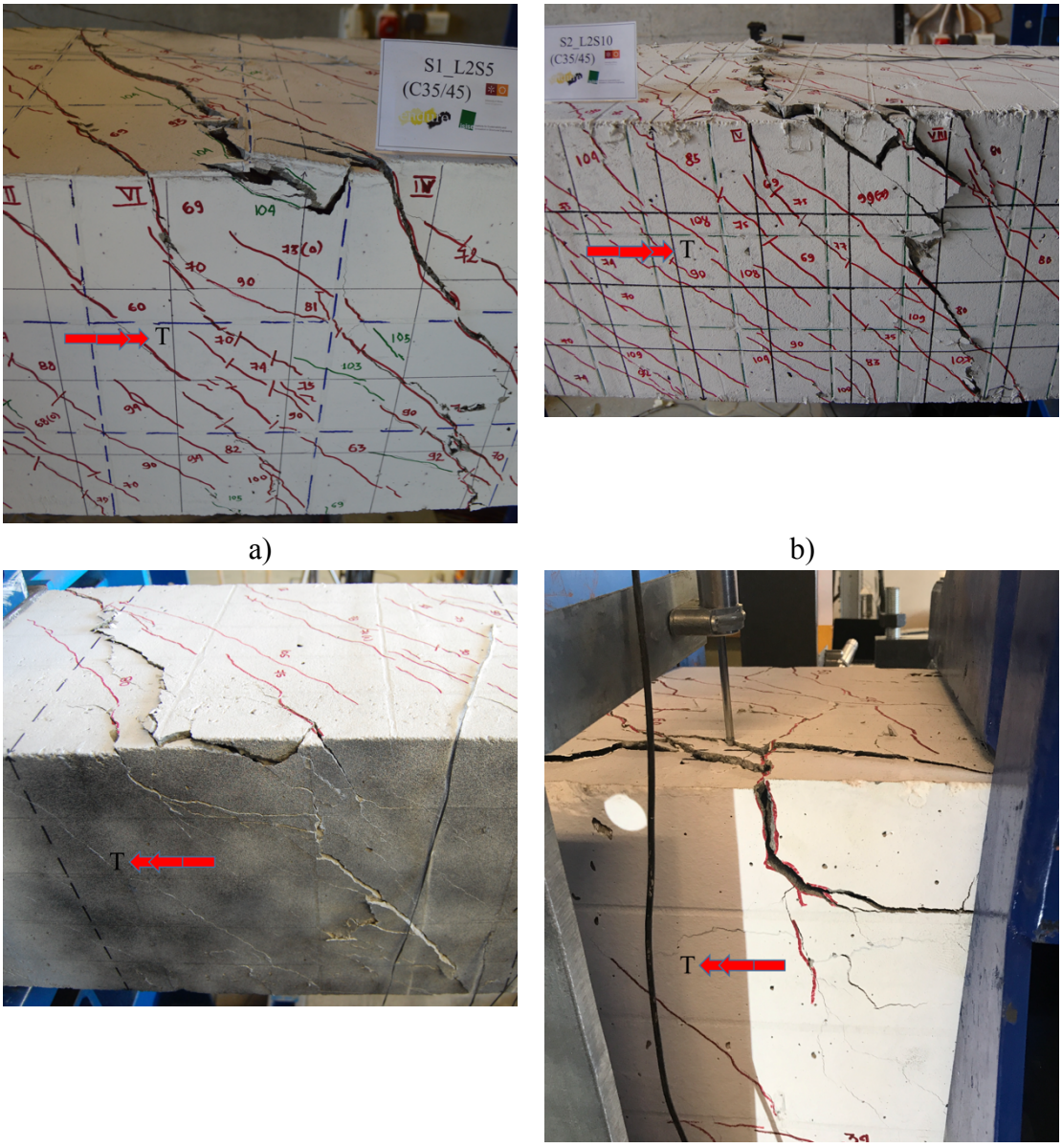

a) b)

c) d)

Fig. 16 - Failure configuration of beam: a) S_L2S5; b) S_L2S10; c) S_L4S5; and d) S_L4S10

List of Tables

Table 1 - Details of beams, reinforcement and strengthening ratios and spacing

Beam	A_{sl} (mm^2)	ρ_{sl} (%)	ρ_{fl} (%)	$\rho_{l,eq}$ (%)	A_{sw} (mm^2)	ρ_{sw} (%)	ρ_{fw} (%)	$\rho_{w,eq}$ (%)	s_{fl}	s_{fw}
S_L2S5 (Fig. 3a)	628	0.571	0.096	0.667	50.24	0.502	0.071	0.573	134	65
S_L2S10 (Fig. 3b)	628	0.571	0.096	0.667	50.24	0.502	0.141	0.644	134	40
S_L4S5 (Fig. 3c)	628	0.571	0.192	0.763	50.24	0.502	0.071	0.573	80	65
S_L4S10 (Fig. 3d)	628	0.571	0.192	0.763	50.24	0.502	0.141	0.644	80	40

Table 2 - Location of linear variable displacement transducers (LVDT) according to the coordinate system XYZ represented in Fig 3

	X (mm)	Y (mm)	Z (mm)
LVDT 1	400	200	350
LVDT 2	350	200	0
LVDT 3	0	200	50
LVDT 4	50	200	400
LVDT 5	150	350	0
LVDT 6	250	50	0
LVDT 7	200	350	1900

Table 3 - Properties for the steel reinforcements

Property	ϕ8 (mm)	COV (%)	ϕ10 (mm)	COV (%)
Modulus of elasticity, E_{sm} (GPa)	195.98	0.45	205.73	10.25
Yield stress, f_{ym} (MPa)	566.71	7.45	449.49	2.69
Yield strain, ε_{ym} ($\mu\varepsilon$)	3.06	11.53	2.46	22.87
Tensile strength, f_{um} (MPa)	680.27	4.74	560.99	1.48

Table 4 - Experimental results of the tested beams in terms of torsional moment

Beam	$M_{t,cr}$ (kN·m)	$\left(\frac{M_{t,cr}^{S}-M_{t,cr}^{R}}{M_{t,cr}^{R}}\right)$	$M_{t,A}$ (kN·m)	$M_{t,syi}$ (kN·m)	$\left(\frac{M_{t,syi}^{S}-M_{t,syi}^{R}}{M_{t,syi}^{R}}\right)$	$M_{t,p}$ (kN·m)	$\left(\frac{M_{t,p}^{S}-M_{t,p}^{R}}{M_{t,p}^{R}}\right)$
Ref_4S	28.01	-	40.02	47.29	-	56.69	-
S_L2S5	25.04	-10.61	41.99	55.23	16.79	78.30	38.11
S_L2S10	28.46	1.64	48.26	57.63	21.87	81.69	44.09
S_L4S5	34.41	22.87	50.27	56.40	19.27	79.37	39.99
S_L4S10	39.26	40.17	55.18	59.39	25.58	83.02	46.43
CoV.	18.42%		13.11%	8.47%		14.31%	

$M_{t,cr}^{S/R}$: S and R stand for, respectively, strengthened and reference beam

Table 5 - Experimental results of the tested beams in terms of angle of rotation and torsional stiffness

Beam	$\theta_{t,cr}$ (deg)	$\left(\frac{\theta_{t,cr}^{S}-\theta_{t,cr}^{R}}{\theta_{t,cr}^{R}}\right)$	$\theta_{t,A}$ (deg)	$\theta_{t,syi}$ (deg)	$\left(\frac{\theta_{t,syi}^{S}-\theta_{t,syi}^{R}}{\theta_{t,syi}^{R}}\right)$	$\theta_{t,p}$ (deg)	$\left(\frac{\theta_{t,p}^{S}-\theta_{t,p}^{R}}{\theta_{t,p}^{R}}\right)$
Ref_4S	0.39	-	0.54	2.77	-	4.78	-
S_L2S5	0.33	-14.43	0.57	2.76	-0.44	7.31	53.01
S_L2S10	0.30	-23.20	0.50	2.57	-7.24	8.40	75.83
S_L4S5	0.62	59.28	0.92	2.94	5.97	8.23	72.21
S_L4S10	0.78	101.88	1.14	2.97	7.22	8.19	71.43
CoV.	43.16%		38.49%	5.73%		20.54%	

$\theta_{t,cr}^{S/R}$: S and R stand for, respectively, strengthened and reference beam

Table 6 - Experimental results of the tested beams in terms of torsional stiffness

Beam	$k_{t,lin}$ (kN·m/deg)	$\left(\frac{k_{t,lin}^{S}-k_{t,lin}^{R}}{k_{t,lin}^{R}}\right)$	$k_{t,Mcr}$ (kN·m/deg)	$\left(\frac{k_{t,Mcr}^{S}-k_{t,Mcr}^{R}}{k_{t,Mcr}^{R}}\right)$	$k_{t,syi}$ (kN·m/deg)	$\left(\frac{k_{t,syi}^{S}-k_{t,syi}^{R}}{k_{t,syi}^{R}}\right)$
Ref_4S	69.80	-	4.02	-	7.36	-
S_L2S5	64.46	-7.66	5.77	43.64	6.10	-17.06
S_L2S10	87.30	25.07	5.97	48.60	7.69	4.58
S_L4S5	45.08	-35.41	3.74	-7.03	7.49	1.81
S_L4S10	48.43	-30.61	3.42	-14.84	6.20	-15.76
CoV.	27.16%		26.10%		10.87%	

$k_{t,cr}^{S/R}$: S and R stand for, respectively, strengthened and reference beam

Table 7 - Location of linear strain gauges(SG's) according to the coordinate system XYZ represented in Fig 5a

Strain gauge (SG)	X (mm)	Y (mm)	Z (mm)
SG_LS1	200	950	367
SG_TS1	200	850	375
SG_LS2	33	950	200
SG_TS2	25	850	200
SG_LF1	135	950	380
SG_TF1	200	915	390
SG_LF2	20	950	265
SG_TF2	10	985	200

LS – SG on longitudinal steel reinforcement; TS – SG on transverse steel reinforcement;
LF – SG on longitudinal CFRP laminate; TF – SG on transverse CFRP laminate

Table 8 - Evolution of steel strains at yielding initiation of steel reinforcement ($\theta_{t,syi}$), torsional strength ($\theta_{t,p}$) and ultimate torsional angle ($\theta_{t,u}$).

Beam	Strain gauges	Strain at $\theta_{t,syi}\left(\mu\varepsilon\right)$	Strain at $\theta_{t,p}\left(\mu\varepsilon\right)$	Strain at $\theta_{t,u}\left(\mu\varepsilon\right)$
Ref_4S	SG_LS1	-6847	-5536	-5087
	SG_TS1	1244	19825	19825
	SG_LS2	-	-	-
	SG_TS2	-213	471	16069
S_L2S5	SG_LS1	1592	1479	1233
	SG_TS1	-	-	-
	SG_LS2	-	-	-
	SG_TS2	-	-	-
S_L2S10	SG_LS1	2757	606	20327
	SG_TS1	717	941	1434
	SG_LS2	1882	2005	2185
	SG_TS2	1210	1322	18063
S_L4S10	SG_LS1	1569	2488	2331
	SG_TS1	2129	2420	2376
	SG_LS2	1827	2140	2107
	SG_TS2	717	807	807

Table 9 - Evolution of CFRP strains at yielding initiation of steel reinforcement ($\theta_{t,syi}$), torsional strength ($\theta_{t,p}$) and ultimate torsional angle ($\theta_{t,u}$).

Beam	Strain gauges	Strain at $\theta_{t,syi}(\mu\varepsilon)$	Strain at $\theta_{t,p}(\mu\varepsilon)$	Strain at $\theta_{t,u}(\mu\varepsilon)$
S_L2S5	SG_LF1	2302	4120	4120
	SG_TF1	3093	5771	5771
	SG_LF2	680	1190	1190
	SG_TF2	2632	4581	4581
S_L2S10	SG_LF1	2796	6214	10977
	SG_TF1	3624	8013	6937
	SG_LF2	62	6043	6385
	SG_TF2	986	5397	6054
S_L4S5	SG_LF1	112	7188	6621
	SG_TF1	1095	11046	10426
	SG_LF2	4023	7032	6535
	SG_TF2	102	5927	5379
S_L4S10	SG_LF1	641	2635	2685
	SG_TF1	2528	3914	3950
	SG_LF2	12	909	933
	SG_TF2	-102	1543	1572

Table 10 – Average crack spacing (s_{rm}) and average crack orientation (α_{crm}) of the tested beams

Beam	Average crack spacing s_{rm} (mm)	$\frac{s_{rm}^{S} - s_{rm}^{R\_4S}}{s_{rm}^{R\_4S}}.100$	Average crack orientation, α_{crm} (degrees)
Ref_1S	412	-	50
Ref_4S	200	-	50
S_L2S5	133	34	51
S_L2S10	104	48	54
S_L4S5	133	33	49
S_L4S10	101	49	49

s_{rm}^{S/R_4S} : S and R stand for strengthened and reference beam, respectively